Hyper-velocity stars from globular clusters hosting intermediate-mass black holes

Matilda Skantz

Division of Astrophysics
Department of Physics
Lund University

2023-EXA207

Degree project of 15 higher education credits
June 2023

Supervisor: Abbas Askar

Division of Astrophysics
Department of Physics
Box 43
SE-221 00 Lund
Sweden

Abstract

In 1988 Hills proposed that stars can gain velocities above 500 $\mathrm{km\,s^{-1}}$ if they are in a stellar binary which gets disrupted by a super massive black hole (SMBH). One of the stars would get trapped in an elliptical orbit around the SMBH while the other gets ejected and obtains a relatively high velocity. Normally stars within galaxies have low peculiar velocities but stars ejected with velocities over 500 $\mathrm{km\,s^{-1}}$ can potentially escape the galaxy. Stars of this nature are called hypervelocity stars (HVS) and in 2005 the first of such a star was discovered in the halo of our Galaxy.

For this project we study the possibility of HVSs being generated by the less established intermediate-mass black hole (IMBH). There is some evidence, while not concrete, suggesting that IMBHs can exist in globular clusters (GCs) making this the environment we are considering. We set up and study the outcome of about 100,000 scattering encounters between a stellar binary and an IMBH for a range of different initial conditions. Not only do we analyze the interactions that result in the production of a high-velocity star due to the Hills mechanism but also the ones resulting in mergers and flybys. All of this is performed using the `Tsunami` code which is an N-body integrator with a lot of useful tools and features.

We reach the conclusion that the semi-major axis of the stellar binary is the main factor in determining whether or not an HVS can be generated. Of significant importance is also the mass of the IMBH and the initial orientation of the interaction. In addition, mergers occur more frequently when the semi-major axis is tighter and flybys are more likely when the ratio between the pericenter distance of the encounter and the binary semi-major axis is larger. Finally, we obtain 6 HVSs out of 27 encounters between binary white dwarfs and an IMBH for which the initial conditions were taken from realistic GC models.

Populärvetenskaplig beskrivning

En klar natt kan man se tusentals stjärnor på natthimlen ovan oss. Det finns dock mer struktur bakom dem än vad bara ögat kan se. Dessa stjärnor befinner sig oftast i en större grupp med stjärnor kallade stjärnhopar. Det finns stjärnhopar med allt från tio till hundra tusentals stjärnor. De sistnämnda stjärnhoparna är oftast de äldsta och är så kallade klotformiga stjärnhop. Dessa har en kärna där majoriteten av stjärnorna är samlade väldigt tätt inpå varandra vilket gör det till en optimal miljö för interaktion mellan dem. Interaktionerna sker på grund av något vi kallar dynamik som inom astronomin ofta refererar till gravitationen som gör att objekt rör sig. Denna gravitation är densamma som håller kvar våra fötter på jorden och påverkar allt i universum som har en massa. När dynamiska interaktioner uppstår i en stjärnhop kan vi få binära stjärnsystem som består av två stjärnor som snurrar runt varandra, liknande hur vår jord snurrar runt solen.

Efter en lång tid som stjärna, vanligtvis miljoner år, kan massiva stjärnor kollapsa och avsluta sina liv som svarta hål. Svarta hål är kategoriserade efter massa och det finns två tydliga kategorier. Den ena är svarta hål med massor upp till några tiotals den av vår sol medan den andra kategorin är från hundra tusen till miljoner gånger solmassan. I intervallet mellan har vi inga konkreta bevis för svarta hål och därmed ingen definitiv förklaring till deras formation. Dock finns det indikationer på dess existens och en av teorierna är att de kan formas genom en krock av två mindre svarta hål. Med detta i åtanke, är klotformiga stjärnhop en möjlig plats för mellanliggande svarta hål.

I detta kandidatarbete undersöks vad som sker ifall ett binärt system närmar sig ett mellanliggande svart hål i ett klotformigt stjärnhop. Detta utförs genom data simulationer som använder sig av en redan etablerad kod med justeringar för våra egna omständigheter. Undersökningen fokuserar på de hastigheter som kan uppnås när det binära systemet slits isär av den dynamiska interaktionen med det svarta hålet. Normalt sett har stjärnor en hastighet på några tiotals $\mathrm{km\,s^{-1}}$ men genom denna interaktion hoppas vi kunna producera stjärnor med hastigheter över 500 $\mathrm{km\,s^{-1}}$. De initiala omständigheterna för dessa typer av hastigheter, såsom avstånd mellan stjärnorna och massa på det svarta hålet, kommer också att analyseras.

Tidigare har Hills mekanismen blivit väl undersökt under omständigheterna av ett supermassivt svart hål. Den typen av svarta hål vi undersöker är dock inte lika etablerad då bevis för dessa inte är lika övertygande. Om projektet lyckas kan det vara en möjlighet att våra simuleringar jämförs med dokumenterade observationer av höghastighetsstjärnor och på så sätt fastställa deras ursprung. Utöver det kan projektet upplysa oss om sannolikheten att svarta hål med mellanliggande massa existerar och bildas i klotformiga stjärnhop.

Contents

Chapter 1

Introduction

1.1 Runaway and hypervelocity stars

The majority of stars within galaxies like the Milky Way (MW) are located in a galactic disc and exhibit relatively low peculiar velocities. For instance, the velocity dispersion of stars in the solar neighbourhood is a few tens of $\mathrm{km\,s^{-1}}$ (see Table 1.2 in Binney & Tremaine, 2008). Stars with velocities substantially higher than the typical velocity of most stars in a galaxy can be classified as high-velocity stars. Depending on their velocities and the mechanism by which they acquired those velocities, high-velocity stars are often further categorised as either hypervelocity stars (HVSs) or runaway stars (RSs).

RSs are mostly massive stars (O and B-type) with velocities greater than 40 $\mathrm{km\,s^{-1}}$. According to Brown (2015) there are two main ways by which RSs acquire their velocities: supernova explosion in binaries and dynamical ejections. Supernova ejection occurs when one of the stars in a binary system explodes as a supernova. This can result in the companion star getting ejected from the binary with a high-velocity (Blaauw, 1961). The velocity acquired by the RS depends on the supernova kick velocity and the orbital velocity of the progenitor binary. Stars from such interactions can reach a velocity of up to 400 $\mathrm{km\,s^{-1}}$ but most ejections have significantly lower velocities (Brown, 2015). Dynamical ejections occur most often in a young star cluster where the RSs are ejected by dynamical 3- or 4-body-interactions. In this case, the maximum velocity of the ejected star is determined by the escape velocity of the most massive star in the interaction. While velocities can reach up to 600 $\mathrm{km\,s^{-1}}$, the majority of dynamically ejected RSs have velocities of less than 200 $\mathrm{km\,s^{-1}}$ (Perets & Šubr, 2012).

HVSs on the other hand can have velocities in excess of 500 $\mathrm{km\,s^{-1}}$. This value is comparable to the escape velocity of the MW estimated from the observation of stars in the solar neighbourhood (Koppelman & Helmi, 2021). The proposed mechanism by which HVSs acquire their velocities is through a dynamical 3-body interaction between a binary star system and a supermassive black hole (SMBH). This mechanism (also

known as Hills mechanism, see Section 1.1.1) for producing HVS was proposed by Hills (1988) who had predicted that HVS could exist before any of them were actually detected.

In 2005, an HVS with a radial velocity of $\sim$ 850 $\mathrm{km\,s^{-1}}$ was discovered in the halo of our Galaxy at a distance of 55 kpc (Brown et al., 2005). The observed velocity of this HVS is almost twice the Galactic escape velocity and is also higher than the escape velocity from the surface of the star. Such a high velocity cannot be explained by the mechanisms responsible for producing RS (Brown, 2015). Therefore, it is likely that this HVS was produced in a dynamical interaction with a massive black hole (BH) as proposed by Hills (1988). This discovery led to targeted surveys to search for HVS in our Galaxy. The 6.5m Multiple Mirror Telescope (MMT) in Arizona has helped in identifying 42 B-type stars (with masses ranging from $\sim 2-5$ $\mathrm{M_\odot}$) that have radial velocities in the Galactic rest-frame exceeding +275 km $\mathrm{s^{-1}}$ (Brown et al., 2014; Kreuzer et al., 2020). With precision astrometry with *Gaia*, it is now also possible to complement radial velocity measurements of HVSs with accurate measurements of proper motion and distance to them (Brown et al., 2018; Kreuzer et al., 2020). These measurements can be useful for obtaining trajectories of unbound stars in order to better understand their origin. Hattori et al. (2018) used *Gaia* DR2 archival data to identify about 30 HVSs that had observed space velocities $\gtrsim$ 480 km $\mathrm{s^{-1}}$ and had ages and metallicities that are consistent with populations of globular cluster. Furthermore, data from *Gaia* DR3 has also been used to identify a few tens of HVS white dwarfs with inferred velocities larger than 400 $\mathrm{km\,s^{-1}}$ (Igoshev et al., 2023).

In this project, we investigate whether we can obtain high-velocity stars (particularly HVSs with velocities larger than 500 $\mathrm{km\,s^{-1}}$) through 3-body encounters between an intermediate-mass black hole (IMBH) of $10^2 - 10^4$ $\mathrm{M_\odot}$ and a binary star system. As such, the type of star that we want to study could be classified as either an HVS in a sense that we have an interaction with a BH or a RS in the sense that it is a dynamical interaction that does not involve an SMBH ($\gtrsim 10^6$ $\mathrm{M_\odot}$). From here on out we will nonetheless use HVS as we are basing our study on the Hills mechanism discussed in the section below.

1.1.1 The Hills Mechanism

Hills (1988) proposed that an HVS can be produced through an interaction between a tightly bound binary and an SMBH ($\sim 10^6$ $\mathrm{M_\odot}$) at the center of our Galaxy. The basic idea behind the Hills mechanism is that if a binary gets sufficiently close to a massive BH, it can get tidally disrupted which results in one of the stars in the binary being captured around the SMBH in a wide eccentric orbit while the other star gets ejected at a high velocity making it an HVS (see Fig. 1.1). Hills (1988) carried out numerical simulations of 3-body encounters in which a stellar binary with a semi-major axis value of 0.01 AU with component masses of 1 $\mathrm{M_\odot}$ encounters a massive BH (with masses

ranging between $10^4 - 10^7$ $M_\odot$). The results from his work showed that an HVS of up to ~ 4000 km s^{-1} could be produced in an interaction between a binary and a 10^6 $M_\odot$ SMBH. This mechanism was proposed at a time when there was no conclusive evidence for the existence of an SMBH in the center of our Galaxy. Hills (1988) suggested that the detection of such an HVS from the Galactic center could be definitive evidence for the existence of an SMBH. An HVS with a velocity of 4000 km s^{-1} can travel up to a distance of 40 kpc within 10 Myr.

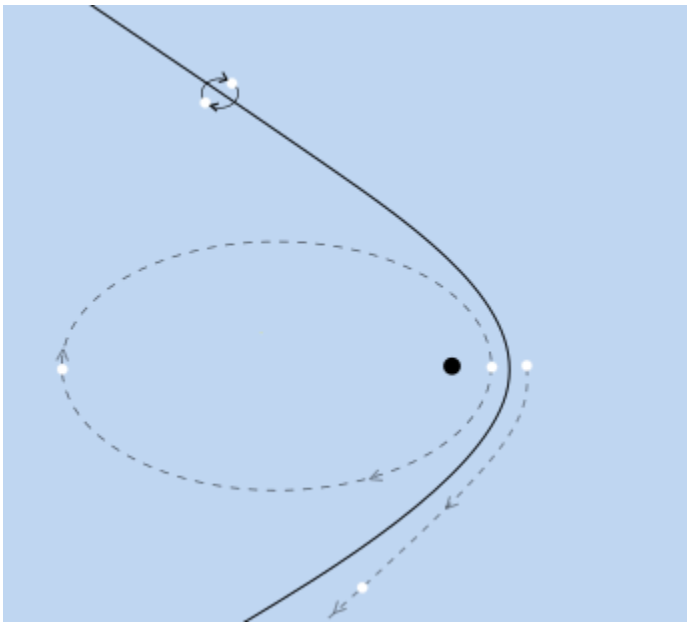

Figure 1.1: Figure illustrating the Hills (1988) mechanism. A close binary system is approaching an SMBH on a parabolic trajectory. If the pericenter distance of this encounter is less than the tidal disruption radius then the binary is disrupted. This results in one of the stars becoming gravitationally bound to the SMBH on an eccentric orbit while the other star is ejected as an HVS.

As the binary approaches the massive BH, the gravitational force exerted on the binary component closer to the BH is stronger than the force on the binary component which is further away. The difference between this force on the binary component is the tidal force. The tidal disruption or splitting radius of a binary star system depends on the separation between its components and the ratio between the mass of the BH and the mass of the binary:

$$r_t \simeq \left(\frac{M_{bh}}{m_1 + m_2}\right)^{1/3} a_{bin} \tag{1.1}$$

where m_1 and m_2 are the masses of the binary components, a_{bin} is the binary semi-major axis and M_{bh} is the BH mass.

In a parabolic encounter, the velocity at the pericenter is equal to the escape velocity at that point. Therefore, in a parabolic encounter between a binary and a massive BH, the velocity of the binary center ($v_{\rm bcm}$) of mass at a pericenter distance equal to the r_t in eq. 1.1 is given by:

$$v_{\rm bcm} = \sqrt{\frac{2GM_{bh}}{r_t}} \tag{1.2}$$

Thus, as the binary approaches the massive BH, its $v_{\rm bcm}$ will depend on the BH mass and the disruption radius of the binary. This $v_{\rm bcm}$ is significantly larger than the orbital velocity of the binary which is given by

$$v_{\rm orb} = \sqrt{\frac{G(m_1+m_2)}{a_{bin}}} \tag{1.3}$$

As the binary is tidally disrupted, one of the stars becomes bound to the massive BH and a result of energy conservation, the other star is ejected at velocity which is roughly equivalent to the geometric mean of $v_{\rm bcm}$ and $v_{\rm orb}$.

Bromley et al. (2006) carried out simulations of 3-body encounters to investigate the ejection velocities produced by the Hills mechanism. Their initial setups were similar to simulations carried out by Hills (1988) with their binaries having no eccentricities and initial velocity at infinity of 250 $\mathrm{km\,s^{-1}}$. The initial parameters sampled by Bromley et al. (2006) took a range of values for m_1 between $3-4$ $\mathrm{M}_\odot$, m_2 between $0.5-4$ $\mathrm{M}_\odot$ and a_{bin} between $0.05-4$AU. The M_{bh} was fixed to be $3.5\times10^6 M_\odot$ for all interactions. The pericenter distance of the encounter ranged between $\sim 1-700$ AU. Bromley et al. (2006) used results from these simulations to show that the velocity of an HVS ejected by the Hills mechanism can be approximated with

$$v_{ej} = 1760\left(\frac{a_{bin}}{0.1\ \mathrm{AU}}\right)^{-1/2}\left(\frac{m_1+m_2}{2\mathrm{M}_\odot}\right)^{1/3}\left(\frac{M_{bh}}{3.5\cdot10^6\mathrm{M}_\odot}\right)^{1/6} f_R \tag{1.4}$$

where f_R is a tuning factor close to one. Its purpose is to tune the ejection speed and is given by

$$f_R = 0.774+(0.0204+\{6.23\cdot10^{-4}+[7.62\cdot10^{-6}+(-4.24\cdot10^{-8}+8.62\cdot10^{-11}D)D]D\}D)D. \tag{1.5}$$

Here, D is the Hills parameter and is defined as

$$D = \frac{q}{a_{bin}}\left(\frac{2M_{bh}}{10^6(m_1+m_2)}\right)^{-1/3} \tag{1.6}$$

where q is the closest distance between the binary and the black hole also known as the pericenter distance. Hills (1988) defines this parameter as a dimensionless closest approach parameter where the factors within the brackets compensates for the increase

in the tidal disruption radius as the mass of the black hole decreases. If the masses of the stars in the binary are not equal, the expected velocities for each mass is

$$v_1 = v_{ej}\left(\frac{2m_2}{m_1+m_2}\right)^{1/2} \quad \text{and} \quad v_2 = v_{ej}\left(\frac{2m_1}{m_1+m_2}\right)^{1/2} \tag{1.7}$$

depending on which binary component becomes the HVS.

From eq. 1.4, it can be seen that tighter binaries can produce higher ejection velocities via the Hills mechanism (Guillochon & Loeb, 2015) since these binaries have larger $v_{\rm orb}$ as shown in eq. 1.3. Furthermore, it can also be seen from eq.1.4 that the velocity of the HVS produced via the Hills mechanism also depends on the mass of the BH, with more massive BHs producing HVS with higher velocities. Therefore, if we replace the SMBH with an IMBH (with masses between 10^2-10^3 $M_\odot$), we can expect that the velocity of the ejected star will be lower.

While galaxies typically have one SMBH in the centers, it has been suggested that IMBHs could form at the center of dense and massive globular clusters (see Section 1.2). Therefore, a galaxy could contain a sizeable number of IMBHs lurking at center of some globular clusters. Encounters between binary stars and an IMBH at the center of a globular cluster could potentially generate HVS via the Hills mechanism.

1.2 Globular clusters and IMBH formation

1.2.1 Dynamical evolution of globular clusters

Globular clusters (GCs) are gravitationally bound collections of typically 10^5 to 10^6 stars that orbit around their host galaxy. These star clusters are supported against gravitational collapse by the internal random orbits of stars which also explains their nearly spherical appearance. GCs in our Galaxy can be dated back to 13 billion years ago and are therefore some of the oldest astronomical objects in the Universe (Karttunen et al., 2017). In the MW alone, there are about 150-200 GCs (Harris, 1996, 2010) but extragalactic GCs have also been observed (Brodie & Strader, 2006). The giant elliptical galaxy M87 has over 10 000 GCs (Benacquista, 2013).

The metallicity, specifically the iron content, of the stars in an individual GC tend to be the same. This is an indicator that most of them were created at the same time as a result of the collapse of the molecular cloud which produced the cluster. Moreover, the colour-magnitude diagram of most GCs provides a distinct main-sequence turn-off which strengthens the argument of the stars mostly being the same age (Benacquista, 2013).

GCs have a characteristic core-halo structure and often have high core densities of up to 10^5 to 10^6 stars per cubic parsec. Outside of the core, the stellar density is much lower. The GCs in our galaxy have typical core radii of about 1 pc and diameters of up to several tens of pc (Benacquista, 2013; Baumgardt & Hilker, 2018). Due to the high densities in the core, close encounters between stars can occur. These close encounters can produce large changes in their velocity. As a result, the gravitational field of the GC fluctuates continuously, further changing the direction and magnitude of the velocity of each individual star within the cluster. Distant encounters have less of an influence on the change in velocity but occur significantly more often. Therefore both types of encounters are an important part of the dynamical evolution of these stellar systems (Spitzer, 1987).

Furthermore, dynamical encounters in the cores of dense star clusters can also lead to the formation of exotic stellar objects (Benacquista, 2013; Davies, 2013). For instance, mergers between stars can occur due to close gravitational encounters and this can lead to the formation of blue straggler stars (BSS). Binary star systems can dynamically form through encounters between three single stars. Binary-single and binary-binary encounters can change properties of existing binaries and can also change membership of binary components via exchange encounters. Such encounters can contribute to the formation of close binary systems containing compact objects (e.g., X-ray binaries, double white dwarf binaries, binary BHs).

Stellar binaries

Stellar binaries are stellar systems where two stars orbit each other or rather a common center of mass. There are two main ways a stellar binary can be created. One is simply that they start off that way when they are "born" and the other is that they become that way through dynamical encounters. If they are starting out as a binary, the evolution of the stars can be influenced by each other if the separation between them is small enough. If they are further apart the stars can evolve independently as usual (Hurley et al., 2002).

The observed present-day binary fraction in GCs is around 10-20% (Milone et al., 2012; Ji & Bregman, 2013; Giesers et al., 2019) while younger, less dense open stellar clusters seem to have a much higher fraction. By analysing the population of O-type stars in Galactic open stellar clusters, Sana et al. (2012) found that about 70% of them are found in binary systems. Therefore, it is possible that a significant number of initial binaries can get disrupted due to dynamical encounters within star clusters. In dynamical encounters, 'soft' binaries can be disrupted. These are binaries for which the binding energy of the binary is less than the mean kinetic energy of cluster stars:

$$\frac{Gm_1m_2}{2a_{bin}} < \frac{1}{2}\langle m\rangle\sigma^2 \tag{1.8}$$

where m_1 and m_2 are masses of the stars in the binary, a_{bin} is the semi-major axis of the binary, $\langle m\rangle$ is the average mass and σ is the velocity dispersion of stars in the GC.

In dynamical encounters, components in these binaries can gain kinetic energy from the interacting star and disrupt the binary. 'Hard' binaries for which the binary binding energy is larger than the mean kinetic energy of cluster stars on the other hand are more likely become harder due to dynamical encounters with surrounding stars (Heggie, 1975; Hills, 1975). Therefore, a higher fraction of 'hard' binaries can survive in a cluster and many observed GC show an increase of binary fraction in their cores (Milone et al., 2012; Giesers et al., 2019).

Intermediate-Mass Black holes

When discussing BHs, we often divide them into two well-observed categories depending on their mass. The first are stellar-mass BHs which, as the name suggest, have masses of up to 50 $M_\odot$. The second category would be SMBHs, these have with masses between $10^6 - 10^{10}$ $M_\odot$(Greene et al., 2020). However, there is a mass range in between these two that is not accounted for and BH in this mass range are called IMBHs and are the main focus of this thesis.

IMBHs are defined as BH with masses in the range of 10^2 to 10^5 $M_\odot$. Concrete evidence for their existence has alluded observers. However, it has been suggested (Greene et al., 2020) that since stellar mass BHs are created by the death of massive stars and we have evidence of SMBHs, IMBHs must have existed at some point in time in order for SMBHs to exist.

Even though there is no concrete evidence of IMBHs (in the mass range $10^3 - 10^4$ $M_\odot$) there are findings that indicate their existence. In 2020, the LIGO-Virgo-KAGRA scientific collaboration announced the discovery of GWs from a binary BH merger which a low-mass IMBH. In this merger event, GW190521, a ~ 150 $M_\odot$ IMBH formed from the merger of a ~ 100 $M_\odot$ and ~ 50 $M_\odot$ BH (Abbott et al., 2020). Another strong indication for the existence of an IMBH is the reported observation of a luminous X-ray burst caused by the tidal disruption of a star by a 20,000 $M_\odot$ IMBH in an extragalactic star cluster (Lin et al., 2018; Wen et al., 2021). Another contributor to the evidence of IMBHs are HVS. In particular, there has been an observation of an HVS which could have been ejected from the Large Magellanic Cloud (LMC). According to Erkal et al. (2018) the star (HVS3) is much more likely to be coming from the LMC than the Galactic center and suggests that the origin should be from a black hole with mass of $4 \cdot 10^3 - 10^4$ $M_\odot$ (Gualandris & Portegies Zwart, 2007).

One of the proposed channels for IMBH formation is through stellar collisions between massive stars in the cores of dense star clusters. If these collisions can occur on timescales less than the evolution time of the stars then a very massive star ($\gtrsim 300$ $M_\odot$) can be built up in the cluster center through runaway collisions. Depending on how this massive star evolves, it is possible that it could collapse into an IMBH. To trigger IMBH formation there should be a sufficiently high number density of stars early in the lifetime of the cluster. Results from numerical simulations of dense star clusters

show that low-metallicity star clusters with initial central densities $\gtrsim 10^6$ $M_\odot$ pc^3 are most likely to trigger IMBH ($\sim 10^2$-10^4 $M_\odot$) formation through this pathway (Portegies Zwart. et al., 2004; Greene et al., 2020; Rizzuto et al., 2021).

If not through stellar collisions, an IMBH could also form in dense star clusters from the repeated mergers of stellar-mass BHs. These types of BHs are created when massive stars ($M_{\rm birth} \gtrsim 20$ $M_\odot$) evolve. A cluster with more than a million stars could contain up to 1000 stellar-mass BH progenitors. Once multiple BHs have been produced through stellar evolution in a cluster they could sink to the cluster core where they can form binaries together. If the resulting binary is tight enough, it could be possible for the BH to spiral in and merge through the gravitational wave radiation (Miller & Hamilton, 2002; Davies, 2013). If the merged BH can be retained in the cluster it could grow further by merging with other BHs (Rodriguez et al., 2019) and this could lead to the formation and growth of an IMBH. While this formation pathway does not require extremely high initial central densities, it does requrie that a sizeable number of stellar BHs are retained in the cluster following their formation.

If an IMBH can form in a GC through one of the channels mentioned above then it could frequently interact with the hard stellar binaries that are observed in the cores of GCs. Therefore, there is a possibility that HVS could be produced through the Hills mechanism in such interactions. While evidence for the existence of an IMBH at the center of Galactic GCs has been controversial (Greene et al., 2020), inferred upper limits on IMBH mass range between few 10^2 $M_\odot$ to $\sim 10^4$ $M_\odot$ (Tremou et al., 2018; Baumgardt et al., 2019).

1.3 Physical Importance and Aim

The aim of the project is to explore whether or not potential IMBHs in GCs can generate HVSs when they undergo close encounters with a stellar binary. By conducting data simulations, we investigate the essential conditions for the formation of an HVS and identify the initial parameter that plays the most significant role. Moreover, the project seeks to investigate the efficacy of the Hills mechanism in the context of close gravitational encounters between a stellar binary and an IMBH in a GC.

Not only does the project consider if an HVS can be produced in this type of three-body encounter, we also analyze what sort of velocities we can obtain for HVS and how they depend on initial parameters of the encounter. Only a few studies (e.g., Pfahl, 2005; Fragione & Gualandris, 2019; Šubr et al., 2019) have investigated HVS production via interactions with an IMBHs in the center of GCs. In this work, we explore a wide range of the initial parameter space by checking how HVS production varies with changing IMBH mass, binary component masses, eccentricity of the binary, and semi-major axis of the binary. Additionally, collision rates and other types of tidal disruptions are to be assessed. Also of interest is the importance of tides in the outcomes.

By studying such encounters, we may be able to predict the properties and rates of HVS stars generated from interactions with IMBHs. This may enable comparison with observations of HVS to perhaps constrain their origin and also shed light on whether GCs are likely to form and contain IMBHs.

Chapter 2

Method

We investigate the production of HVSs in binary-single scattering encounters using numerical simulations that solve the Newtonian gravitational equations of motion (see eq. 2.1) for three bodies. This is done by using the `Tsunami` code that is a direct few-body code which can be used to simulate small-N gravitational dynamics.

$$\ddot{\mathbf{r}}_i = -G \sum_{j \neq i} \frac{m_j \left(\mathbf{r}_i - \mathbf{r}_j\right)}{\left|\mathbf{r}_i - \mathbf{r}_j\right|^3} \tag{2.1}$$

2.1 The Tsunami code

To simulate our scattering experiments, we are using the `Tsunami` code (Trani & Spera, 2023). `Tsunami` is an N-body integrator which uses techniques like regularization of the equations of motion and chain coordinates to accurately compute the outcome of few-body interactions. Regularization introduces a modification to the equations of motion to address the singularity in the gravitational potential as the distance between objects approaches zero (Trani & Spera, 2023). Using chain coordinates can help in minimizing round-off errors that would normally occur with the use of center-of-mass (COM) coordinates in hierarchical systems. This can be important for computing the outcome of scattering encounters in which two bodies are close to each other but far from the center of a global coordinate system, as is the case with the center of mass reference frame in our simulations. `Tsunami` makes use of the concept of ARchain (Mikkola & Aarseth, 1993) which makes a chain of interparticle vectors. The aforementioned vectors are formed between all bodies at every time-step and are sorted by length, starting with the smallest one, to produce the chain. When the system is evolving the order of the chain is updated so that it keeps the smallest vector as the first segment and the second as the one closest to it and so on. Instead of using COM transformations the chain system expresses each body relative to their nearest neighbour on the chain (Atallah et al., 2023).

The code also simplifies the set up with built in functions such as `KeplerUtils` where

one can provide Keplerian orbital elements and transform them into Cartesian coordinates and vice versa. Furthermore, `Tsunami` allows for the inclusion of post-Newtonian corrections to the equations of motion which can account for orbital energy losses due to gravitational wave emission during close encounters between compact objects (Trani et al., 2022). In addition, the code also has options to account for orbital energy losses due to tidal dissipation (Hellström et al., 2022).

2.2 Initial set up for binary star & IMBH encounter

We wanted to set up a two body hyperbolic encounter between an IMBH and the COM of a stellar binary such that the pericenter distance for this encounter is less than the tidal disruption radius:

$$r_t = \left(\frac{m_{\rm imbh}}{m_{\rm bin}}\right)^{1/3} a_{\rm bin}(1 + e_{\rm bin}) \tag{2.2}$$

where $m_{\rm imbh}$ is the mass of the IMBH, $m_{\rm bin}$ is the mass of the binary ($m_{\rm bin} = m_1 + m_2$) and $a_{\rm bin}$ and $e_{\rm bin}$ are the binary semi-major axis and eccentricity. In the next subsection, we describe the theory of hyperbolic orbits and how it was used to help set up our initial conditions.

2.2.1 Hyperbolic trajectory

There are four different types of orbits a body can have based on conic sections. These include circular, elliptical, parabolic, and hyperbolic orbits and are defined by their eccentricity e according to Table 2.1. For our project we chose for the binary to approach the IMBH on a hyperbolic orbit as it is initially unbound to it.

Orbit	Eccentricity
Circular	0
Elliptic	< 1
Parabolic	1
Hyperbolic	> 1

Table 2.1: Eccentricities of different orbits.

Fig. 2.1 shows the different parameters of the orbit. One of them is the pericenter distance q, which is the closest distance between the binary and IMBH during the encounter. Another is the impact parameter b which is the distance between the asymptote of the hyperbolic and the parallel line intersecting the IMBH. We can also observe the semi-major axis a which in the case for hyperbolic orbits is negative in contrast to that of circular or elliptical orbits. Finally we have the semi latus rectum p and as shown in Fig. 2.1, this is the distance between the IMBH and where the line orthogonal to the pericenter intersects the orbit.

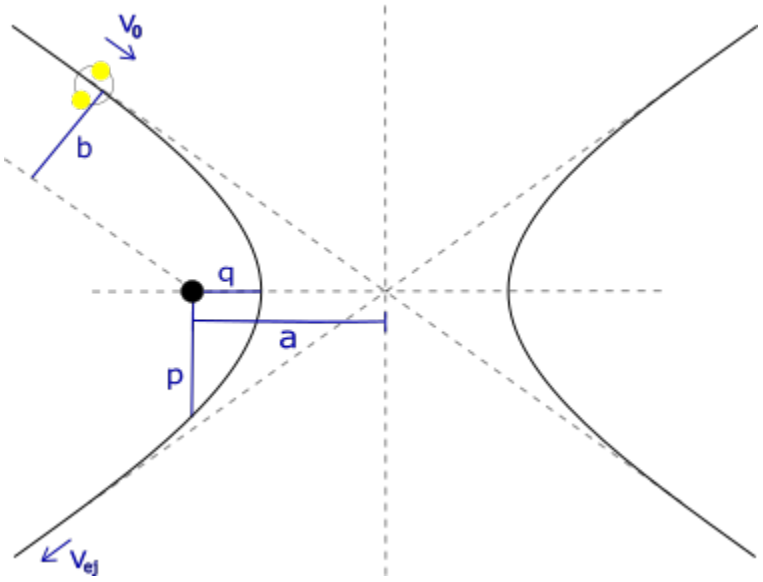

Figure 2.1: Hyperbolic orbit with impact parameter b, pericenter distance q and semi-major axis a. The incoming velocity is v_0 and the velocity of the outgoing HVS is v_{ej}.

For hyperbolic orbits, the semi- latus rectum is given mathematically by

$$p = |a(e^2 - 1)| \tag{2.3}$$

where a is the semi-major axis shown in 2.1. Furthermore, the pericenter distance q is given by

$$q = a|e - 1|. \tag{2.4}$$

In order to determine the semi-major axis (a), eccentricity (e) and true anomaly (ν) of the hyperbolic encounter such that the q is less than r_t in eq. 2.2, we followed along Quillen (2020). The true anomaly is the angular parameter that determines the position of the binary in the hyperbolic orbit and can therefore be used to determine the distance between the bodies. For Keplerian orbits, the distance (d) between the orbiting bodies is given by eq. 2.5:

$$d = \frac{p}{1 + e\cos(\theta - \overline{\omega})} \tag{2.5}$$

where

$$p \equiv \frac{h}{G(m_{\rm imbh} + m_{\rm bin})} \tag{2.6}$$

The d here is the distance between the bodies, θ is the deflection angle, and M and m are masses of the IMBH and binary. h is angular momentum per unit mass and $\overline{\omega}$ in this case is the angle of minimum d which is called longitude of pericenter. $\theta - \overline{\omega}$ can

also be described as the true anomaly ν. As such, the true anomaly of the hyperbolic orbit becomes

$$\nu = \arccos\left(\frac{\frac{p}{d} - 1}{e}\right) \tag{2.7}$$

Combining 2.3 and 2.6 then gives

$$e^2 - 1 = \frac{h^2}{G(m_{\rm imbh} + m_{\rm bin})a} \tag{2.8}$$

The next step is to determine what the semi-major axis of the hyperbolic orbit a should be in terms of v_∞. Following, Quillen (2020) we do this by considering energy conservation, the velocity of the common center of mass of the interaction is given by

$$V_{com} = \frac{m_{\rm bin}}{m_{\rm imbh} + m_{\rm bin}} v_\infty \tag{2.9}$$

where v_∞ is the initial velocity of the binary COM coming towards the fixed mass $m_{\rm imbh}$. The initial total energy is simply the kinetic energy $E = \frac{m_{\rm bin} v_\infty^2}{2}$ and should be equal to the sum of the kinetic energy for the center of mass and the Keplerian energy of the system

$$E = \frac{m_{\rm bin} v_\infty^2}{2} = (m_{\rm bin} + m_{\rm imbh})\frac{V_{com}^2}{2} - \frac{G m_{\rm imbh} m_{\rm bin}}{2a} \tag{2.10}$$

Substituting V_{com} with eq 2.9 results in

$$\frac{m_{\rm bin} v_\infty^2}{2} = \frac{(m_{\rm bin} + m_{\rm imbh})}{2} \frac{m_{\rm bin}^2}{(m_{\rm bin} + m_{\rm imbh})^2} v_\infty^2 - \frac{G m_{\rm imbh} m_{\rm bin}}{2a}$$

$$\Downarrow$$

$$a = -\frac{G(m_{\rm imbh} + m_{\rm bin})}{v_\infty^2} \tag{2.11}$$

Let's now use eq. 2.11 in eq. 2.8

$$e^2 - 1 = \frac{h^2 v_\infty^2}{G^2(m_{\rm imbh} + m_{\rm bin})^2} \tag{2.12}$$

Quillen (2020) also states that $h = b v_\infty$ allowing us to get our eccentricity for the hyperbolic orbit

$$e = \sqrt{\frac{b^2 v_\infty^4}{G^2(m_{\rm imbh} + m_{\rm bin})^2} + 1} \tag{2.13}$$

To summarise, we have expressed the semi-major axis a, the true anomaly ν, our eccentricity e of the encounter in terms of the initial velocity at infinity (v_∞), impact parameter (b), masses $m_{\rm bin}$ and $m_{\rm imbh}$ and the initial distance d.

For each encounter that we simulate, the maximum value of the impact parameter b is determined in such a way that the pericenter distance q which it gives corresponds to r_t in eq. 2.2. Under the assumption of gravitational focusing, when v_∞ is much smaller than the velocity at pericenter, the impact parameter is related to the pericenter distance by:

$$b_{max} = q \cdot \left(1.0 + \frac{2G(m_{\rm imbh} + m_{\rm bin})}{v_\infty^2 q}\right)^{1/2} \tag{2.14}$$

As we want to make sure to keep the interaction within the tidal disruption radius, and thereby not only have flybys, we set $q = r_t$.

2.2.2 Initial Conditions for Encounters

We needed to provide `Tsunami` with the initial x,y,z position coordinates and vx, vy, vz velocity coordinates for each of the 3 objects (2 stars in the binary and an IMBH). We developed a function that takes an input parameter the masses of the stars in the binary (m_1 and m_2), the semi-major axis (a_{bin}) and eccentricity of the binary (e_{bin}), the IMBH mass ($m_{\rm IMBH}$), the relative velocity at infinity (v_∞ or $\rm v_0$) between the binary CoM and the IMBH and the initial distance between the binary COM and IMBH (d). Using these input parameters, we obtain the initial position and velocity coordinates for each objects in two steps. Firstly, we convert Keplerian orbital elements for the binary to Cartesian coordinates to find the center of mass position and velocity coordinates of the binary. To accomplish this, we set the Keplerian orbital elements of the binary (ν_{bin}, i_{bin}, ω_{bin}, Ω_{bin}) randomly within appropriate intervals. These parameters and their intervals can be seen in Table 2.2.

In the second step, knowing the mass of all three objects and v_∞, we determine the semi-major axis of a hyperbolic encounter between the binary COM and the IMBH using eq. 2.11. Next, we determine the maximum impact parameter b_{max} using eq. 2.14. We then randomly pick the actual impact parameter by uniformly sampling between 0 and b_{max}^2. Knowing the actual impact parameter b, we use eq. 2.13 to find the eccentricity of the encounter. Finally, knowing the eccentricity and the initial distance of our setup, we can calculate ν using eq. 2.7. The initial distance for each encounter was to 1000 times the value of a_{bin}. The inclination (i), argument of periapsis (ω) and Longitude of ascending node (Ω) for the encounter between the binary COM and the IMBH are randomly sampled in the appropriate ranges (see Table 2.2). We convert these Keplerian orbital elements for the hyperbolic encounter to Cartesian coordinates. We can then easily compute the 3D position and velocities for each star in the COM reference frame of the interaction.

Parameter		Span
True anomaly	ν_{bin}	$0, 2\pi$
Inclination	i_{bin}	$\arccos(-1, 1)$
Inclination	i	$\arccos(-1, 1)$
Argument of periapsis	ω_{bin}	$0, 2\pi$
Argument of periapsis	ω	$0, 2\pi$
Longitude of ascending note	Ω_{bin}	$0, 2\pi$
Longitude of ascending note	Ω	$0, 2\pi$
Impact parameter	b	$0, b_{max}$

Table 2.2: All of the randomized parameters and their range. Subscript *bin* indicates that it is for the binary while no subscript means it is for the hyperbolic orbit between the binary COM and the IMBH.

Furthermore, the longitude of the ascending node for both the hyperbolic orbit and the binary orbit was set to zero if the inclination $i < 1 \cdot 10^{-8}$ while the argument of the periapsis for both orbits was set to zero if the eccentricity $e < 1 \cdot 10^{-8}$. Otherwise the aforementioned parameters were randomized between 0 and 2π as listed in Table 2.2. These parameters influence the initial orientation of the interaction and set the initial position of the three objects. Therefore, they are picked randomly to ensure a statistically representative sample of possible encounter configurations.

Parameters such as mass, semi-major axis of the binary, and eccentricity of the binary are expected to be related to the velocity of the HVS produced in these encounters. To investigate their impact, we set these to be of one value for 5000 simulations and create an output file for later analyzing. For the initial runs, we carried out 16 sets of 5000 Hills mechanism encounters setting IMBH mass and binary semi-major axis value to the ones shown Table 2.3 while the eccentricity of the binary was set to zero.

Mass IMBH ($M_\odot$)	Semi-major axis a_{bin} (AU)
100	0.02
500	0.05
1000	0.5
5000	1

Table 2.3: Varied values of the initial 16 runs of 5000 interactions. Stellar masses were 1 $M_\odot$ each, e_{bin}=0.0, and v_∞=10 km s^{-1}.

After performing the initial 16 runs, three additional runs of 5000 encounters were done where the eccentricity of the binary was changed to 0.2, 0.5, and 0.7. The mass of the IMBH and semi-major axis of the binary were kept at 1000 $M_\odot$ and 0.05 AU respectively.

To further confirm that the v_∞ of the binary does not influence the expected HVS, runs with both higher (50 $\mathrm{km\,s^{-1}}$) and lower (5 $\mathrm{km\,s^{-1}}$) velocity than 10 $\mathrm{km\,s^{-1}}$ at infinity, were carried out. Once again the semi-major axis and mass of the IMBH was kept constant at the same values as previously.

For the last simulations of 5000 the scenario with two different masses in the binary was considered. We performed runs where m_1 was kept constant at 1 $\mathrm{M_\odot}$ while m_2 was changed to 5, 10, and 20 $\mathrm{M_\odot}$. The standard case of $e = 0$, $v_\infty = 10$ $\mathrm{km\,s^{-1}}$, $m_{IMBH} = 1000$ $\mathrm{M_\odot}$, and $a = 0.05$ AU was otherwise kept constant. One of the main reasons for performing these runs are to allow us to assess eq. 1.7.

Main-sequence Binaries

We start this project with main-sequence binaries in mind. Essentially, this means that all of the runs previously mentioned are being executed with stars of 1 $\mathrm{M_\odot}$ and radii of 1 $R_\odot$ unless explicitly stated otherwise. With this radius we decided that a_{bin} should not be less than 0.02 AU for our initial runs in order to avoid too many mergers. For runs where the mass of the stars in the binary was changed, the radius was determined using the mass-radius relation from Demircan & Kahraman (1991).

White Dwarf Binaries

As a second part of the project, we simulated about 27 binary-single encounters between a binary white dwarf system and an IMBH ($M > 100$ $\mathrm{M_\odot}$) taken from GC models that were simulated for the MOCCA-Survey Database I project (Askar et al., 2017) using the Monte Carlo N-body code, MOCCA (Hypki & Giersz, 2013). These binary-single encounters were selected because their outcome had resulted in an exchange. We re-simulated these encounters with `Tsunami` to see whether these encounters could have produced an HVS. Accordingly, radii, masses, initial velocity, a_{bin}, and the impact parameter were all taken from the MOCCA data for these encounters. Since white dwarfs are more compact than main-sequence stars they have a significantly smaller radius and thus allow for more compact binaries without resulting in collisions. The setup for these encounters was on a planar orbit and we only simulated each encounter once.

2.3 Simulation Data and Analysis

`Tsunami` can be run through a few different interfaces and for this project its Python interface was chosen. By following along with a couple of examples from `Tsunami` we then wrote our own Python code. Once we had the initial set-up, described in the section above, an output file with initial parameters as well as final parameters and the resulting velocities was created. We had one main output file which was set up to record 5000 interactions that resulted in one of the stars being bound to the IMBH

while the other gets ejected. If an interaction resulted in a merger, flyby, or both stars in the binary being either unbound or bound to the IMBH, the output was recorded into separate output files for each scenario and was not counted towards the 5000 interactions. This was accomplished by setting conditions for the semi-major axis of both the inner and outer orbit.

Each encounter was simulated with `Tsunami` up to a final time T where $T = d/v_\infty$. d is the initial distance between the binary COM and the IMBH which was typically set to 1000 times the value of the binary semi-major axis. v_∞ was the relative velocity at infinity which was set to $10\mathrm{km\,s^{-1}}$ for most interactions. This value is consistent with the velocity dispersion of stars in GCs (Fragione & Gualandris, 2019). Setting the final time to d/v_∞ ensured that we had pericenter passage and the ejection of the HVS. The position and velocities of the objects at the final time were used to identify the HVS and determine its velocity. In the cases where we had a collision between two objects before the final time, Tsunami would stop the encounter and provide information about which two objects had collided. A collision is recorded when the distance between two objects is less than the sum of their radii. The radii of IMBHs in our setup was determined by calculating their Schwarzschild radius ($r_s = \frac{2GM_{\mathrm{IMBH}}}{c^2}$).

Chapter 3

Results

As a first indication of whether our orbits had been set up correctly we plotted the trajectories of each of the bodies in the interaction as well as the disruption radius around the black hole. For clarity the example shown in Fig. 3.1 was kept in the xy-plane with no inclination. The IMBH mass was 1000 $M_\odot$ and the binary masses were 1 $M_\odot$ each. In the top right corner is the incoming binary, with $a_{bin} = 0.05$ AU and $v_\infty = 10\ \mathrm{km\,s^{-1}}$, where the blue and red line represent each star's trajectory. When the binary enters the disruption radius the red star is captured in an elliptic orbit around the IMBH and the blue gets ejected at a velocity of 668 $\mathrm{km\,s^{-1}}$. Blue and red in this case does not to represent the type of star as both stars are main-sequence stars with radii of 1 $R_\odot$.

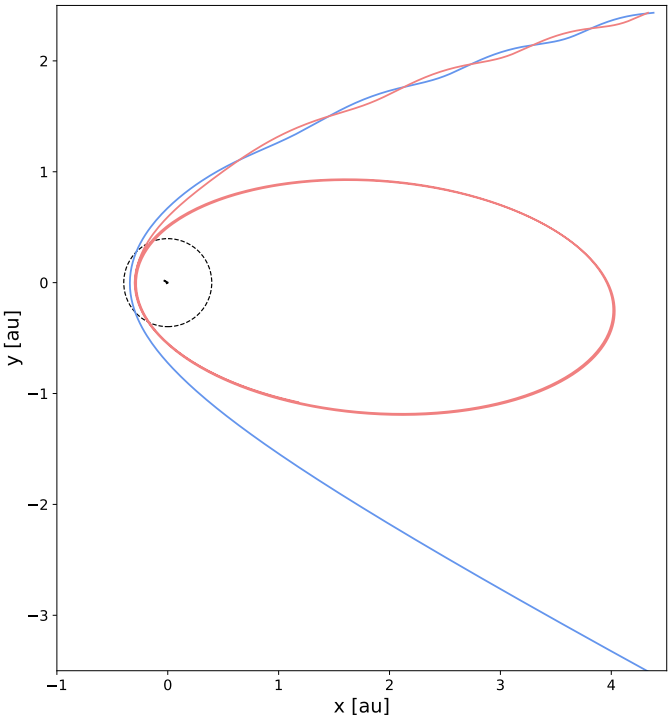

Figure 3.1: Orbit in xy-plane produced by code. For this interaction $a_{bin} = 0.05$ AU, mass of the IMBH was a thousand $M_\odot$ and the stellar masses were 1 $M_\odot$ each. The disruption radius of the IMBH is shown in the dashed circle around it. $v_\infty = 10\,\mathrm{km\,s^{-1}}$ while the velocity of the HVS is $v_{ej} = 668\,\mathrm{km\,s^{-1}}$.

3.1 Velocity Distribution of HVS

3.1.1 Dependence of HVS on initial cluster parameters

The first result from the initial 5000 runs in Table 2.3 gave the velocity distributions in Fig. 3.2 of an IMBH with mass of 1000 $M_\odot$. The mass of each star in the binary is 1 $M_\odot$ and their radius is assumed to be the same as that of our sun. The figure shows the comparison of how the different distances between the binary stellar components affects the out coming velocities of the ejected star. As expected a tighter binary will result in higher velocities but not only that, they are much more spread out than the binaries with a larger distance from each other. It is also evident that for an IMBH of 1000 $M_\odot$ there is a high probability of obtaining an HVS with v >500 $\mathrm{km\,s^{-1}}$ if the binary is tight enough. This is clear as $a_{bin} = 0.05$ gives a velocity peak at just over 600 $\mathrm{km\,s^{-1}}$ and $a_{bin} = 0.02$ shows a velocity peak at approximately 1000 $\mathrm{km\,s^{-1}}$. On one of

the histograms a Gaussian fit of the velocities was also performed using `curve_fit` from `scipy_optimize` and compared to the expected velocity from eq. 1.4. In this example, v_{ej} was calculated separately for each of the 5000 interactions and then added up to obtain a mean value, while in the figures after Fig. 3.2 a mean value of the pericenter distance q was simply put in the equation. As one can observe, the theory agrees very well with the result. The mean velocity provided by the fit was 600.99 $\mathrm{km\,s^{-1}}$ and the calculated expected velocity was 600.86 $\mathrm{km\,s^{-1}}$. This seems very promising that our program has been set up and working correctly.

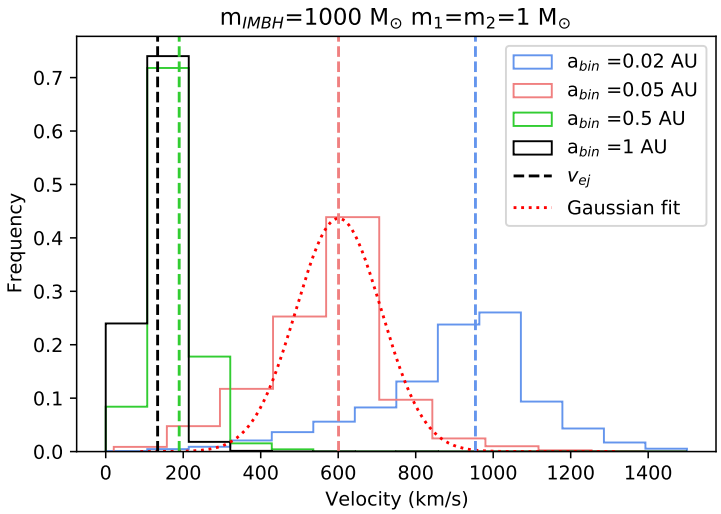

Figure 3.2: Normalized histogram of interactions of Table 2.3 where the mass of the IMBH was 1000 $\mathrm{M_\odot}$, $e_{bin} = 0$, and $v_\infty = 10\,\mathrm{km\,s^{-1}}$. The a_{bin} was varied between four set values and each of those four had 5000 interactions. In the dashed lines we can also observe the calculated theoretical value of v_{ej} from eq. 1.4. On the histogram for $a_{bin} = 0.05$ AU a Gaussian fit of the velocity distribution was performed. This gave a mean value of 600.99 while the calculated v_{ej} is 600.86 $\mathrm{km\,s^{-1}}$.

In Fig. 3.3, the masses and radii of the binary components remain the same while the distance between them is set to 0.05 AU and the mass of the IMBH is varied. The difference between the initial masses of the IMBH does not appear to make as much of a difference as the tightness of the binary but a noticeable one nonetheless. We note velocity peaks at approximately 300 $\mathrm{km\,s^{-1}}$, 600 $\mathrm{km\,s^{-1}}$, 625 $\mathrm{km\,s^{-1}}$ and 800 $\mathrm{km\,s^{-1}}$ for masses 100 $\mathrm{M_\odot}$, 500 $\mathrm{M_\odot}$, 1000 $\mathrm{M_\odot}$ and 1000 $\mathrm{M_\odot}$ respectively. It is also worth mentioning that the theoretical v_{ej} seems to be a better fit for the higher masses than the lower.

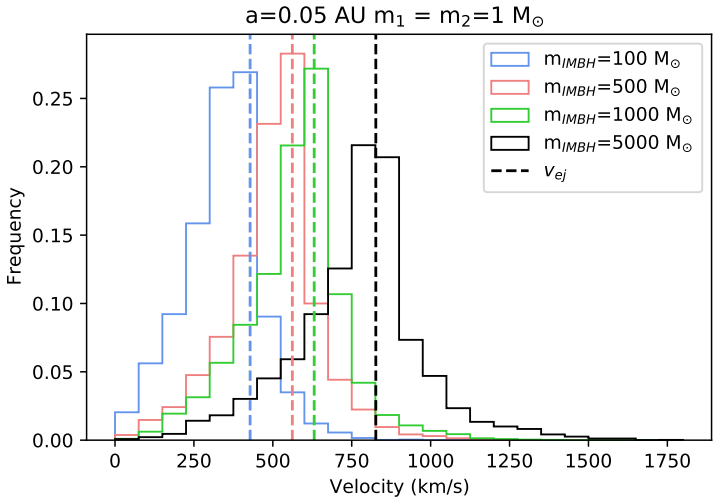

Figure 3.3: Normalized histogram of interactions where the semi-major axis a_{bin} was kept at 0.05 AU. Similarly as before we have $e_{bin} = 0.0$, and $v_\infty = 10\,\mathrm{km\,s^{-1}}$ but this time the mass of the IMBH was varied between four values. Each of these had 5000 interactions once again as explained in Table 2.3.

So far the initial velocity at infinity of the binary COM has been set to 10 $\mathrm{km\,s^{-1}}$ and the eccentricity has been set to 0. From eq. 1.4 we do not expect these parameters to have a significant impact on the velocity of the HVS. Fig. 3.4 and 3.5 confirms this somewhat. The change in initial velocity barely cause a noticeable difference while the histograms have slightly higher and sharper velocity peaks when eccentricity is closer to zero. For higher eccentricity values, the binary components spend more time close to the apocenter of the orbit where they are moving slower. This is also the reason why we believe that the simulations with higher eccentricity are more spread out, the distance between the binary components varies more as the eccentricity is increased.

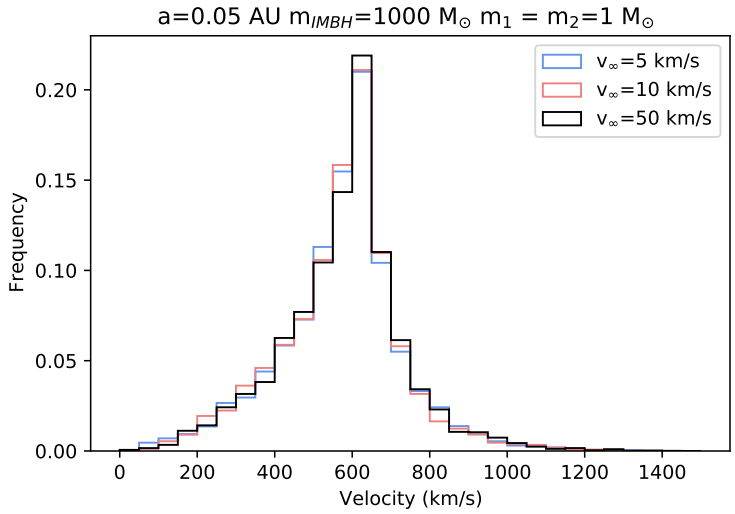

Figure 3.4: Comparison of the change in v_∞. Everything else is kept constant as per usual.

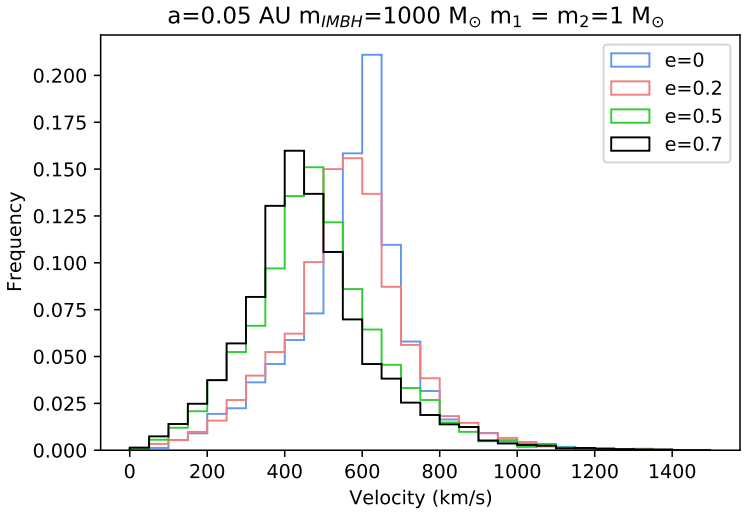

Figure 3.5: Comparison of e_{bin} with constant masses, a_{bin} = 0.05 AU, and v_∞=10 km s^{-1}.

Finally, we were also interested in how the velocities are affected by a ratio between the masses. For this particular set-up we used that the radii of the stars follow the mass-radius relation provided in Demircan & Kahraman (1991); Fragione & Gualandris (2019):

$$\begin{cases} R = 1.06(m_*/\mathrm{M}_\odot)^{0.945} & m_* < 1.66\mathrm{M}_\odot \\ R = 1.33(m_*/\mathrm{M}_\odot)^{0.555} & m_* > 1.66\mathrm{M}_\odot \end{cases} \tag{3.1}$$

The v_{ej} was also changed to the ones given in eq. 1.7 and here as well they seem to

fit better for higher masses as seen in Fig. 3.6. Furthermore, the histogram has been separated by which of the stars ended up as the HVS. There is a clear distinction that the lower masses end up with the higher velocity. Velocity peaks for $m_2 = 5\,\mathrm{M}_\odot$ are at just under 500 $\mathrm{km\,s^{-1}}$ for HVS = m_2 and 1100 $\mathrm{km\,s^{-1}}$ for HVS=m_1. For $m_2 = 10\,\mathrm{M}_\odot$ the velocity peak is slightly lower than that of $m_2 = 5\,\mathrm{M}_\odot$ and approximately 1500 $\mathrm{km\,s^{-1}}$ for HVS=m_1 meaning that the HVSs are significantly faster when the mass ratio is greater. Furthermore, it was expected that we would obtain more HVS with the lower mass rather than the higher but as Table 3.1 show, the difference is not too noticeable. Nevertheless, there is an indication that a greater ratio induces a larger difference.

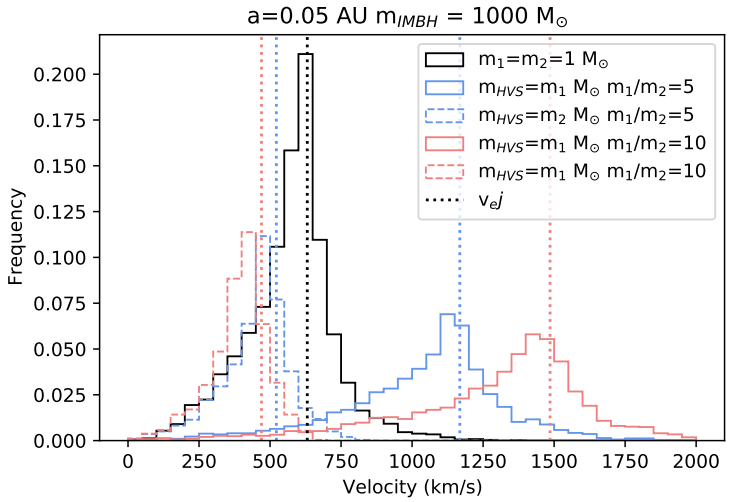

Figure 3.6: Results of a system with a mass ratio between the binary stars. The mass of the IMBH was kept constant at 1000 $\mathrm{M}_\odot$ and a_{bin} was kept constant at 0.05 AU. Eccentricity here was also zero and the v_∞ was 10 $\mathrm{km\,s^{-1}}$. The data has also been separated based on which of the stars that ended up as the HVS. The dashed line symbolizes the heavier of the masses while the regular line is the lighter mass. Dotted line is the expected velocity according to eq. 1.4 and 1.7.

Interactions with a_{bin}=0.05 AU and m_{IMBH} = 1000 $\mathrm{M}_\odot$			
m_1 ($\mathrm{M}_\odot$)	m_2 ($\mathrm{M}_\odot$)	HVS with m_1	HVS with m_2
1	5	55%	45%
1	10	56 %	44%
1	20	59%	41%

Table 3.1: Comparison of which of the stars that got ejected when introducing a difference between the masses of the binary componants.

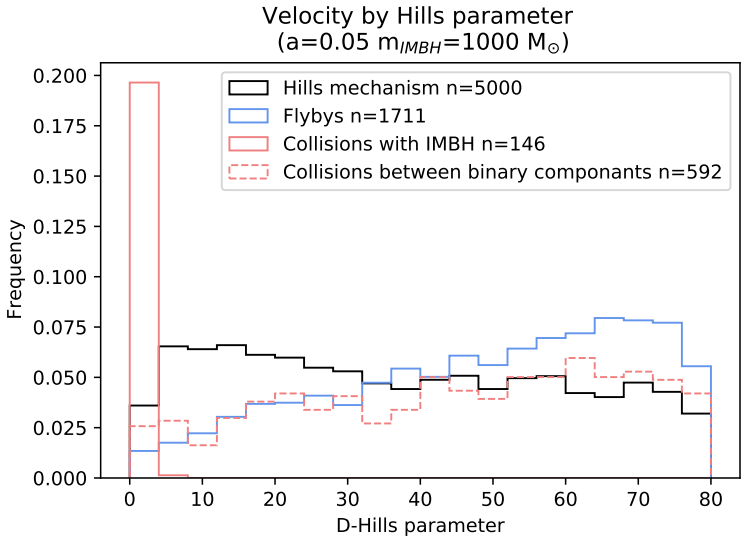

Figure 3.7: Histogram of the normalized Hills parameter for the cases generating the Hills mechanism, the cases generating collisions and the cases generating the flybys. The y-axis therefore represents the fractions of total interactions that resulted in that outcome. The collisions are, in addition, separated by which of the three bodies that collided.

When comparing the Hills parameter we discovered a ratio when $D < 1$ of 80:1 between the interactions resulting in collisions and the interactions resulting in the Hills mechanism. This ratio applies to the standard case $a_{bin} = 0.05$ AU and $m_{IMBH} = 1000\mathrm{M}_\odot$. When the semi major axis instead was lowered to $a_{bin} = 0.02$ there were no interactions where $D < 1$ for the Hills mechanism while 91 interactions resulted in collisions. As there are more cases resulting in the Hills mechanism than the amount of collisions in our simulations it is a good idea to normalize before comparing the ratio to achieve a more accurate representation. Doing that, for $D < 1$, produced the ratios in Table 3.2 below. From Fig. 3.7 it is evident that the ratio declines rapidly after setting a higher limit for D. Due to the Hills parameter being calculated according to eq. 1.6 the only thing that is changing is the pericenter distance q where the first bin in Fig. 3.7 corresponds to $q < 0.2$ AU and the plot showing this can be found in the appendix Fig. C.1. As the histogram is further sorted by which of the bodies that are colliding we can make the conclusion that the closer the binary comes to the IMBH the more likely it is that one of the stars merges with the black hole. There is also a histogram of the Hills parameter for the flybys in Fig. 3.7 and although it is rather obvious it is worth mentioning that these cases more often had higher D-values.

a_{bin} (AU)	Ratio
0.02	Blows up
0.05	542:1
0.5	18.7:1
1	11.9:1

Table 3.2: Comparison between the semi major axis of the binary and the ratio of normalized amount of collisions to the amount of Hills mechanism for $D < 1$. The number on the left are collisions while the right is Hills mechanism. For $a_{bin} = 0.02$ there are no cases with the Hills mechanism but 91 collisions.

Finally, we take a look at how the angle between the incoming binary's orbital angular momentum and the angular momentum of the binary relative to the black hole has an influence on the velocity of the HVS. When they are aligned there should be a greater probability of generating higher velocities than when they are counter-aligned. Fig. 3.8 shows the mean velocities sorted by the angle between the angular momenta and it is evident that the mean velocity decreases as we are moving away from alignment.

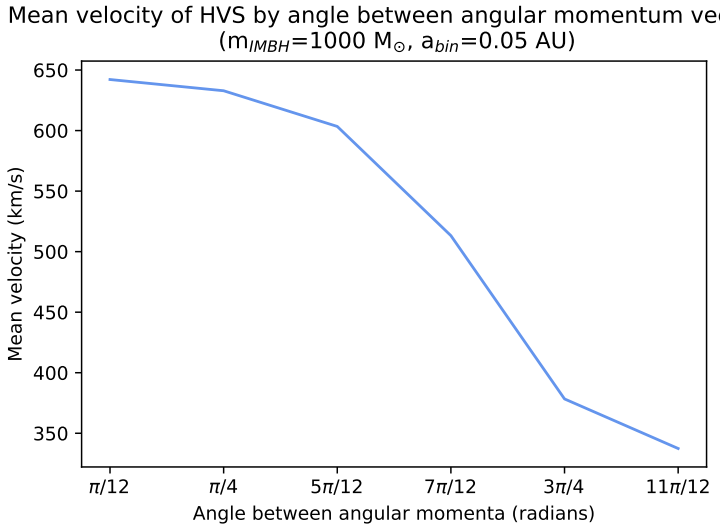

Figure 3.8: Mean velocities of the HVSs sorted by angle between the angular momentum vectors of the orbits. X-ticks show the midpoint value of the interval of angles by which the mean velocity was calculated.

3.2 Merger and Flyby Interactions

After analyzing the main files of the simulations we move on to the encounters that did not result in the Hills mechanism. Table 3.3 shows how many of each type of interaction it took to produce 5000 interactions where an HVS was produced via the Hills mechanism. Mergers between the binary components were, as should be, more

often occurring when the binary was tighter and the mass of the IMBH was larger. Fewer collisions between one of the stars and the IMBH also occurred when the IMBH mass was greater. At first glance, this struck us as a bit peculiar but after some thought we think this might be due to how we are setting up our parameters. Since the span of the impact parameter b_{max} is dependent on the tidal disruption radius, which in turn is dependent on the IMBH mass, this might be one of the reasons we are getting fewer mergers. There were simply more interactions where the binary approached the IMBH further away. This is also somewhat consistent with the amount of flybys although they do not follow as clear of a relation.

Additionally, it turned out that we obtained no interactions where both stars became unbound and no interactions where the intact binary was bound to the IMBH. On the other hand, a few interactions where both the stars of the disrupted binary ended up bound to the black hole did occur. This is most likely a temporary state and not a stable system seeing as there was very few of them. Both stars being bound occurred most often for the lower mass IMBHs suggesting that these are more likely to be stable systems than those with higher mass.

a_{bin} (AU)	IMBH Mass ($M_\odot$)	Mergers	Mergers with star and IMBH	Mergers between binary stars	Both bound	Flybys
0.02	100	3192	986	2206	112	809
	500	2496	468	2028	31	1205
	1000	2293	333	1960	6	1361
	5000	2065	176	1889	2	1325
0.05	100	1155	433	722	162	1184
	500	832	197	635	24	1688
	1000	738	146	592	2	1711
	5000	664	74	590	0	1686
0.5	100	135	45	90	96	2041
	500	110	30	80	8	2024
	1000	114	22	92	4	2019
	5000	91	9	82	3	1931
1	100	67	21	46	60	2089
	500	68	15	53	5	2022
	1000	58	8	50	2	1973
	5000	45	6	39	2	1928

Table 3.3: Summary of the amount of mergers and flybys for each run of 5000 interactions. Corresponds to Table 2.3 in the Method.

`Tsunami` also provides an option for enabling energy losses due to tidal dissipation so this feature was briefly explored. There was no difference in the velocities we obtained or the mergers but a small difference in the amount of flybys of about 1%. The exact

numbers are in Table 3.4. Effects of tides may be more effective for stars with larger radii and perhaps this can be investigated in future works.

a_{bin} (AU)	IMBH Mass ($M_\odot$)	Flybys	Tides enabled
0.05	100	1184	No
		1181	Yes
	500	1688	No
		1684	Yes
0.5	100	2041	No
		2039	Yes
	500	2024	No
		2019	Yes

Table 3.4: When tides were enabled, the amount of mergers and both bound outcomes remained the same as well as the velocities. However, the amount of flybys changed with around 1%.

3.3 Binary WD and IMBH Interactions

The final results from simulating detected white dwarf binaries are shown in Table B.1. In some cases the components were still interacting and the final time was changed to secure an HVS. For most of these interactions the initial distance stayed as $100 \cdot a_{bin}$ but for others this needed to be altered. It turned out that some of the interactions resulted in a fly-by when the distance was $100 \cdot a_{bin}$. To see if the interaction could produce an HVS the initial distance was changed. The aforementioned would change the outcome quite a bit and we managed to get one of the binary components as our HVS for all of the interactions except those which ended in collision. The conclusion is that the position of the stars in the binary (their orbital phase) is important when they enter within the disruption radius. Worth mentioning is also that all of the white dwarf interactions were planar and had zero inclination, ω and Ω values.

In 6 of the 27 interactions, shown in Table 3.5, a velocity greater than 500 $\mathrm{km\,s^{-1}}$ was achieved. Out of these, the greatest velocity was just above 1800 $\mathrm{km\,s^{-1}}$ and the trajectories of that interaction are shown in Fig. 3.9. Given that the initial distance had such a big impact on the outcome, a conclusion on the probabilities is hard to draw. Nevertheless, the possibility of gaining an HVS from white dwarf binaries interacting with an IMBH definitely exists and could potentially account for observed HVS WDs (Igoshev et al., 2023).

Initial parameters										Outcome	
m_1	m_2	m_{IMBH}	a_{bin}	e_{bin}	R_1	R_2	R_{IMBH}	v_∞	b	v_{HVS}	ID HVS
($M_\odot$)			(AU)		($R_\odot$)			(km s^{-1})	(AU)	(km s^{-1})	
0.319328	0.898544	834.503	0.0182548	0	0.0176784	0.00919456	0.0035433	53.3055	7.23355	1803.52	m_1
0.946993	0.905173	427.409	0.0372475	0.429241	0.00865262	0.00912031	0.00181478	35.607	4.23433	584.39	m_2
0.822912	0.452955	2006.29	0.0207368	0	0.0100485	0.0149922	0.00851869	127.704	4.90659	1631.98	m_1
0.967101	0.413009	7574.41	0.0101632	0	0.00842761	0.0157025	0.0321609	189.689	0.848301	1048.04	m_1
0.967213	0.731364	243.086	0.0136507	0.000137542	0.00842635	0.0111161	0.00103214	378.691	0.243588	890.00	m_2
0.976836	0.742058	741.416	0.0162052	9.9697e-05	0.0083185	0.0109885	0.00314805	87.2973	1.22778	883.60	m_2

Table 3.5: Summary of the six white dwarfs that generated an HVS. Shown are all of the initial conditions for observed white dwarf binaries as well as the outcome of our simulation.

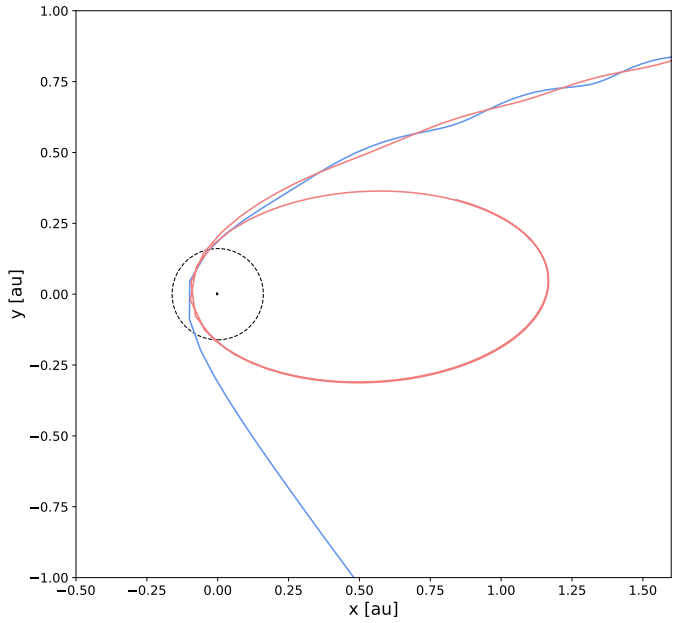

Figure 3.9: Trajectory of the WD binary which produced an HVS of 1803.52 km s^{-1}. The blue is the trajectory of m_1 while the red is of m_2 and we can clearly see that m_1 ends up as the HVS while m_2 gets captured in an elliptic orbit around the IMBH. The tidal radius of the IMBH is shown with the dashed line and the black dot is the position of it. The mass of the IMBH in this case was $m_{IMBH} \approx 800\,M_\odot$ and the semi-major axis of the binary was $a_{bin} \approx 0.018$. More details are shown in the first line in Table 3.5.

Chapter 4

Future Work: Fate of stars ejected from globular clusters via the Hills Mechanism

If there was more time for the project we would have also liked to compare our results with the observed HVS in our Galaxy. In order to demonstrate how this could be done, we generated 5000 HVS generated in binary-single encounters with a 1000 $M_\odot$ IMBH. The masses of the binary components were sampled uniformly between 0.7 - 1.0 $M_\odot$, the eccentricity of the binaries were picked between 0 and 1 from a thermal distribution (uniform in e^2) and the semi-major axis were picked from a uniform in log distribution between 0.01 and 1 AU. The mean value of the HVS star ejected in this sample was 286 $\mathrm{km\,s^{-1}}$. Only 697 out of the 5000 HVSs had ejection velocities larger than 500 $\mathrm{km\,s^{-1}}$ and the highest velocity HVS had a velocity of 1590 $\mathrm{km\,s^{-1}}$.

If we assume that a GC like 47 Tuc (NGC 104) contains an IMBH which is 1000 $M_\odot$ (Kızıltan et al., 2017) and that this IMBH formed 10 Gyr ago and roughly every 2 Myr this IMBH disrupts a binary and ejects out an HVS via the Hills mechanism then we could use our sample of simulated HVS to integrate their orbits from the time of ejection from 47 Tuc up to present day. To try to accomplish this, we used `galpy` [1] (Bovy, 2015) to integrate the orbit of 47 Tuc backwards in time for 10 Gyr in the `MWPotential2014` potential. We transform the orbit of 47 Tuc at that time to the Galactocentric reference frame. Knowing the 3D position and 3D velocity of 47 Tuc at that time, we initialize a new orbit by copying the 3D positions of 47 Tuc and to the vx, vy and vz of the orbit we add the velocity of the first HVS in our sample (projected onto the three dimensions using random angles). We then integrate this HVS 10 Gyr forward in time using `galpy`. We repeat this procedure for the next HVS which is ejected from the cluster 9998 Myr ago and evolved from that time. We do this for all the 5000 HVS that we generated in our sample with the last HVS ejected out of 47 Tuc about 2 Myr. For each of these HVS that were integrated forward in time, we obtain their present-day properties from

[1] available at http://github.com/jobovy/galpy

`galpy`. This approach was taken in a recent paper by Cabrera & Rodriguez (2023) to forward integrate escaping stars from simulated GC models.

Fig. 4.1 shows the Galactocentric x-position and y-position of the orbit of 47 Tuc integrated backwards in time for 10 Gyr. The coloured points show the position in the orbit when an HVS was ejected out of the cluster. The colours indicate the velocities of the HVS ejected by the IMBH through the Hill's mechanism.

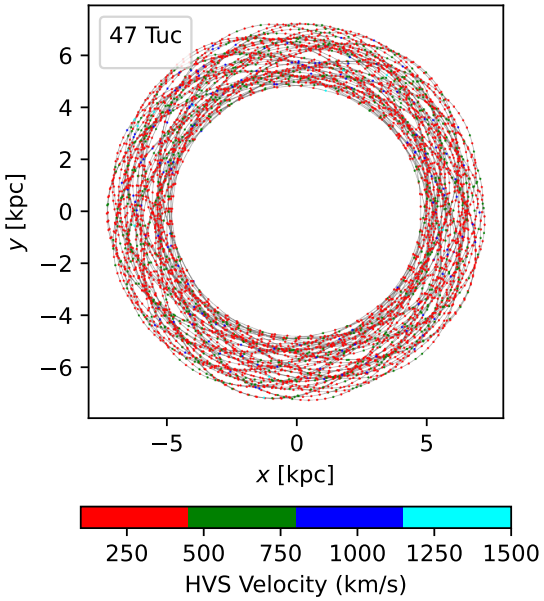

Figure 4.1: X-Y position of the orbit of 47 Tuc integrated 10 Gyr back in time with `galpy`. Points indicate the instance in the orbit when an HVS was ejected from the cluster.

Fig. 4.2 shows an all-sky map in Galactic coordinates for the present-day position of the HVSs that were ejected from 47 Tuc by an IMBH via the Hills mechanism. The colours in the figure indicate the distance from the observer in kpc. HVSs that were ejected out a few Gyr ago can travel up to very far distances with present day distances of up to 10^4 kpc. For a handful of HVSs that were ejected in the last 120 Myr and had Galactic rest frame radial velocities larger than 550 $\mathrm{km\,s^{-1}}$ and present-day Galactocentric distance less than 150 kpc, we plot their trajectories on the sky seen from the current fixed position of the earth in Fig 4.3. The radial velocities and Galactocentric distance of these HVS are comparable to observed HVS (Brown et al., 2018) (see Fig. C.2). However, given that the GCs are old, the masses of the ejected HVSs are considerably lower than the observed HVS identified by Brown et al. (2018). However, this exercise demonstrates that if we have realistic models of a specific GC, we could use this procedure to present-day orbits and positions of HVS that could have been ejected out of a GC by an IMBH.

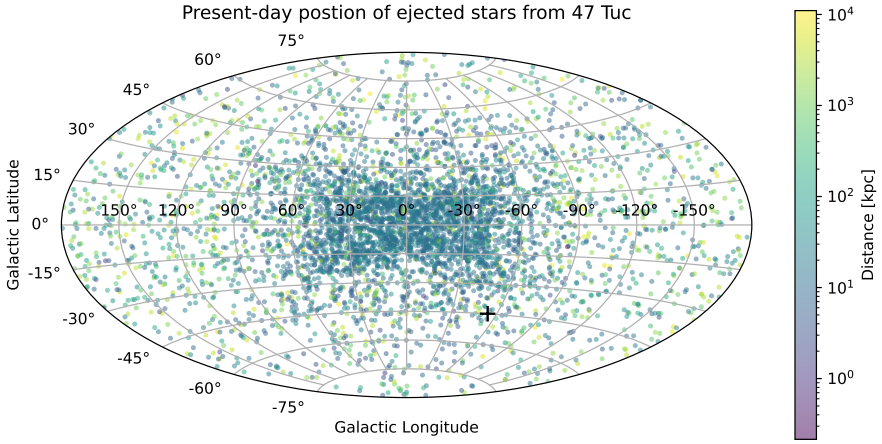

Figure 4.2: All-sky map in Galactic coordinates for the present-day position of the 5000 HVSs that were ejected out from 47 Tuc. The colours of the points represent the distance to the observer in kpc. The plus sign indicates the present-day position of 47 Tuc.

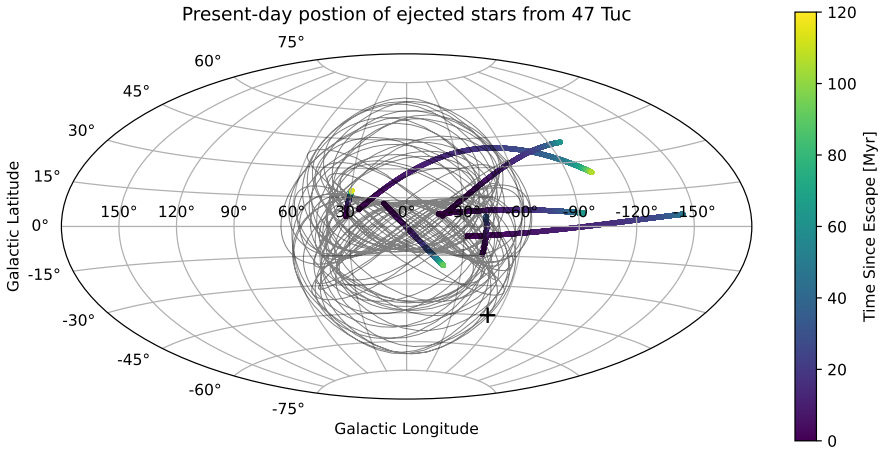

Figure 4.3: All-sky map showing the 10 Gyr back integrated orbit of 47 Tuc (in grey). The trajectories of a few selected HVSs with Galactic rest frame radial velocities larger than 550 $\mathrm{km\,s^{-1}}$ and Galactocentric distance less than 150 kpc are plotted on top of the figure. The coloured points in the trajectories indicate the time since they were ejected from 47 Tuc.

Chapter 5

Conclusions

In this work, we simulated over 100 000 close binary-single encounters between two stars in a binary and an IMBH for a variety of different initial parameters. The efficacy of the Hills mechanism was analyzed by not only saving data from the encounters that resulted in the ejection of an HVS but also keeping track of other possible outcomes that did not generate an HVS. From our work we draw the conclusions that:

- Our simulations agree with the theory and previously presented results (Hills, 1988; Bromley et al., 2006; Fragione & Gualandris, 2019) for the distribution of ejected velocity v_{ej} of an HVS produced via the Hills mechanism.
- For an IMBH with mass of 1000 $M_\odot$ we only generate an HVS when the semi-major axis $a_{bin} \lesssim 0.05$. The typical velocity of $a_{bin} = 0.05$ is approximately 600 $\mathrm{km\,s^{-1}}$ and for $a_{bin} = 0.02$ it is about 1000 $\mathrm{km\,s^{-1}}$.
- For a fixed semi-major axis of $a_{bin} = 0.05$ we generate an HVS for all four IMBH masses. Even though the typical velocity of IMBH mass 100 $M_\odot$ is around 300 $\mathrm{km\,s^{-1}}$ there are some encounters that produce HVSs with velocities exceeding 500 $\mathrm{km\,s^{-1}}$. The other typical velocities are approximately 600, 625, and 800 $\mathrm{km\,s^{-1}}$ for IMBH masses 500, 1000, and 5000 $M_\odot$ respectively.
- When fixing both IMBH mass and semi-major axis to $m_{IMBH} = 1000\,M_\odot$ and $a_{bin} = 0.05$ we see that varying the velocity of the binary at infinity does not impact the velocities of the HVSs.
- When fixing both IMBH mass and semi-major axis to $m_{IMBH} = 1000\,M_\odot$ and $a_{bin} = 0.05$, once again, but instead varying the eccentricity we find some dependence showing that more eccentric binaries produce lower typical velocities but higher maximum velocity. This is most likely due to eq. 1.3 and the fact that the stars spend more time close to apocenter of their orbits where they are moving slower.

- Up until this point the masses of the binary stars have been kept at 1 $M_\odot$ each. When changing the second mass to 5 and 10 $M_\odot$ the typical velocity splits into two, one for m_1 becoming the HVS and one for m_2 becoming the HVS. When the heavier mass m_2 is ejected the typical velocity is just under 500 $\mathrm{km\,s^{-1}}$ for $m_2 = 5$ and a little bit less than that for $m_2 = 10\,M_\odot$. On the other hand, when m_1 is ejected the typical velocities are about 1100 $\mathrm{km\,s^{-1}}$ for $m_2 = 5\,M_\odot$ and just under 1500 $\mathrm{km\,s^{-1}}$ when $m_2 = 10\,M_\odot$. Accordingly, a greater ratio results in the lower mass in the binary being ejected at higher velocities even reaching as high as over 2000 $\mathrm{km\,s^{-1}}$ for a ratio of 1:10.

- The angle between the orbital angular momentum vector of the binary and the angular momentum vector of the binary approaching the IMBH generally generates higher velocities when they are aligned and lower when they are anti-aligned.

- A low periapsis distance of $q < 0.2$ increases the risk of collisions and corollary so does a low Hills parameter of $D < 1$. These numbers apply for $m_{IMBH} = 1000 M_\odot$, $m_1 = m_2 = 1\,M_\odot$ and $a_{bin} = 0.05$ AU.

- Rate of mergers increases when the binary is tighter, i.e when a_{bin} is smaller, and flybys are dependent both on the semi-major axis and mass of the IMBH. As the impact parameter is set up by tidal disruption radius, the collisions involving one star and the IMBH decreased when the IMBH mass was increased. Enabling tides changed the results minimally with only about 1% less flybys.

- Finally, by simulating WD binaries from GC models we find 6 out of the 27 observed WD binaries generated an HVS. While the initial distance greatly influenced the results making the probability of an HVS hard to estimate there is still a definite possibility of an IMBH yielding an HVS from interaction with a WD binary

There are still some directions which this work could be taken in the future. One of them is considering the position of the cluster in our galaxy and evolving HVSs from it to make predictions on where some of the observed HVS might have originated from.

Acknowledgements

First and foremost I want to thank my supervisor Abbas Askar whose genuine excitement on the project motivated me greatly. Not only that but he was also extremely helpful and a pleasure to work with. This project could not have been completed without him. I also want to thank Alessandro Trani for his help with Tsunami and his insight on the computational set-up.

To my fellow bachelor students, Benjamin Dahlén, Filip Gustavsson, Johan Holmberg, Oskar Nilsson, Eric Svensson, Melvin Tham, Elliot Winsnes, and especially Claudia Skoglund, I want to say that I appreciate all the time we have spent together and I am thankful for the encouragements you all have brought me.

Bibliography

Abbott, R., Abbott, T. D., Abraham, S., et al. 2020, ApJ, 900, L13

Askar, A., Szkudlarek, M., Gondek-Rosińska, D., Giersz, M., & Bulik, T. 2017, MNRAS, 464, L36

Atallah, D., Trani, A. A., Kremer, K., et al. 2023, Growing Black Holes through Successive Mergers in Galactic Nuclei: I. Methods and First Results

Baumgardt, H., He, C., Sweet, S. M., et al. 2019, MNRAS, 488, 5340

Baumgardt, H. & Hilker, M. 2018, MNRAS, 478, 1520

Benacquista, Matthew J andDowning, J. M. B. 2013, Living Reviews in Relativity, 16, 4

Binney, J. & Tremaine, S. 2008, Galactic Dynamics: Second Edition

Blaauw, A. 1961, Bulletin of the Astronomical Institutes of the Netherlands, 15, 265

Bovy, J. 2015, ApJS, 216, 29

Brodie, J. P. & Strader, J. 2006, ARA&A, 44, 193

Bromley, B. C., Kenyon, S. J., Geller, M. J., et al. 2006, The Astrophysical Journal, 653, 1194

Brown, W. R. 2015, Annual Review of Astronomy and Astrophysics, 53, 15

Brown, W. R., Geller, M. J., & Kenyon, S. J. 2014, ApJ, 787, 89

Brown, W. R., Geller, M. J., Kenyon, S. J., & Kurtz, M. J. 2005, The Astrophysical Journal, 622, L33

Brown, W. R., Lattanzi, M. G., Kenyon, S. J., & Geller, M. J. 2018, ApJ, 866, 39

Cabrera, T. & Rodriguez, C. L. 2023, arXiv e-prints, arXiv:2302.03048

Davies, M. B. 2013, in Galactic Structure and Stellar, Vol. 5, Planets, Stars and Stellar Systems, ed. T. Oswalt & G. Gilmore (Springer)

Demircan, O. & Kahraman, G. 1991, Astrophysics and Space Science, 181, 313

Erkal, D., Boubert, D., Gualandris, A., Evans, N. W., & Antonini, F. 2018, Monthly Notices of the Royal Astronomical Society, 483, 2007

Fragione, G. & Gualandris, A. 2019, MNRAS, 489, 4543

Giesers, B., Kamann, S., Dreizler, S., et al. 2019, A&A, 632, A3

Greene, J. E., Strader, J., & Ho, L. C. 2020, Annual Review of Astronomy and Astrophysics, 58, 257

Gualandris, A. & Portegies Zwart, S. 2007, MNRAS, 376, L29

Guillochon, J. & Loeb, A. 2015, ApJ, 806, 124

Harris, W. E. 1996, AJ, 112, 1487

Harris, W. E. 2010, arXiv e-prints, arXiv:1012.3224

Hattori, K., Valluri, M., Bell, E. F., & Roederer, I. U. 2018, ApJ, 866, 121

Heggie, D. C. 1975, MNRAS, 173, 729

Hellström, L., Askar, A., Trani, A. A., et al. 2022, MNRAS, 517, 1695

Hills, J. G. 1975, AJ, 80, 809

Hills, J. G. 1988, Nature, 331, 687

Hurley, J. R., Tout, C. A., & Pols, O. R. 2002, Monthly Notices of the Royal Astronomical Society, 329, 897

Hypki, A. & Giersz, M. 2013, MNRAS, 429, 1221

Igoshev, A. P., Perets, H., & Hallakoun, N. 2023, MNRAS, 518, 6223

Ji, J. & Bregman, J. N. 2013, The Astrophysical Journal, 768, 158

Karttunen, H., Kröger, P., Oja, H., Poutanen, M., & Donner, K. J. 2017, Fundamental Astronomy, 6th edn. (Berlin: Springer)

Kızıltan, B., Baumgardt, H., & Loeb, A. 2017, Nature, 542, 203

Koppelman, H. H. & Helmi, A. 2021, Astronomy & Astrophysics, 649, A136

Kreuzer, S., Irrgang, A., & Heber, U. 2020, A&A, 637, A53

Lin, Strader, J., Carrasco, E. R., et al. 2018, Nature Astronomy, 2, 656

Mikkola, S. & Aarseth, S. J. 1993, Celestial Mechanics and Dynamical Astronomy, 57, 439

Miller, M. C. & Hamilton, D. P. 2002, MNRAS, 330, 232

Milone, A. P., Piotto, G., Bedin, L. R., et al. 2012, A&A, 540, A16

Perets, H. B. & Šubr, L. 2012, ApJ, 751, 133

Pfahl, E. 2005, ApJ, 626, 849

Portegies Zwart., Baumgardt, H., Hut, P., Makino, J., & McMillan, S. L. W. 2004, Nature, 428, 724

Quillen, A. 2020, The Hyperbolic orbit, Lecture Notes, aST233-Course Lecture

Rizzuto, Naab, T., Spurzem, R., et al. 2021, MNRAS, 501, 5257

Rodriguez, Zevin, M., Amaro-Seoane, P., et al. 2019, PRD, 100, 043027

Sana, H., de Mink, S. E., de Koter, A., et al. 2012, Science, 337, 444

Spitzer, L. 1987, Dynamical Evolution of Globular Clusters (Princeton, NJ: Princeton University Press), 26

Trani, A. A., Rastello, S., Di Carlo, U. N., et al. 2022, MNRAS, 511, 1362

Trani, A. A. & Spera, M. 2023, IAU Symposium, 362, 404

Tremou, E., Strader, J., Chomiuk, L., et al. 2018, ApJ, 862, 16

Šubr, L., Fragione, G., & Dabringhausen, J. 2019, MNRAS, 484, 2974

Wen, Jonker, P. G., Stone, N. C., & Zabludoff, A. I. 2021, ApJ, 918, 46

Appendix A

List of acronyms

- COM - Center of mass
- GC - Globular cluster
- HVS - Hyper-velocity star
- IMBH - Intermediate-mass black hole
- MW - Milky Way
- RS - Runaway star
- SMBH - Super-massive black hole

Appendix B

Table

Initial parameters										Outcome	
m_1	m_2	m_{IMBH}	a_{bin}	e_{bin}	R_1	R_2	R_{IMBH}	v_∞	b	v_{HVS}	ID HVS
($M_\odot$)			(AU)		($R_\odot$)			($km\,s^{-1}$)	(AU)	($km\,s^{-1}$)	
1.00914	0.826846	115.02	0.502826	0.733012	0.00795508	0.0100036	0.000488374	6.55406	130.286	90.87	m_1
0.319328	0.898544	834.503	0.0182548	0	0.0176784	0.00919456	0.0035433	53.3055	7.23355	1803.52	m_1
0.581326	0.537741	129.112	0.578698	0	0.0130337	0.0136546	0.00054821	19.6984	41.1963	131.61	m_1
0.384102	1.37694	366.416	0.021934	0.804386	0.0162591	0.00281017	0.0015558	9.60605	3.65838	255.00	m_2
0.946993	0.905173	427.409	0.0372475	0.429241	0.00865262	0.00912031	0.00181478	35.607	4.23433	584.39	m_2
0.822912	0.452955	2006.29	0.0207368	0	0.0100485	0.0149922	0.00851869	127.704	4.90659	1631.98	m_1
1.37662	1.36364	17707.1	0.0162851	0.0463719	0.00281753	0.00309988	0.0751844	446.843	0.0649206	Collision	m_1, m_2
0.967101	0.413009	7574.41	0.0101632	0	0.00842761	0.0157025	0.0321609	189.689	0.848301	1048.04	m_1
0.949452	1.29206	240.899	2.5785	0.963969	0.00862512	0.0043741	0.00102286	18.1061	26.5685	36.36	m_2
1.10415	1.10298	155.492	0.212087	0.641115	0.00686097	0.00687478	0.00066022	46.0989	1.88758	245.45	m_1
1.4033	0.347733	190.317	0.080213	0	0.00213362	0.0170222	0.000808085	22.5358	3.56189	173.00	m_1
1.19005	1.23422	283.294	0.717049	0.617322	0.00580591	0.00521917	0.00120287	24.9601	5.33808	72.90	m_2
1.19005	1.23422	283.294	2.17089	0.717082	0.00580591	0.00521917	0.00120287	27.6415	6.44019	51.73	m_2
1.37013	1.02341	370.506	0.134872	0.550659	0.00296175	0.00779354	0.00157317	7.73707	13.5824	28.44	m_2
1.26288	1.06776	1667.01	0.155064	0.755992	0.00481378	0.00728614	0.00707811	77.8914	0.33986	307.14	m_2
0.933738	0.922334	7004.86	0.0355325	0.248058	0.00880082	0.00892831	0.0297426	316.772	0.07589	Collision	m_1, m_{IMBH}
1.12783	1.12736	119.146	0.184706	0	0.00657854	0.00658426	0.000505893	41.277	1.28418	116.01	m_2
0.967213	0.731364	243.086	0.0136507	0.000137542	0.00842635	0.0111161	0.00103214	378.691	0.243588	890.00	m_2
1.0318	0.715966	3967.76	0.0158296	0	0.00769832	0.0113014	0.0168471	115.81	0.127248	Collision	m_1, m_{IMBH}
0.976836	0.742058	741.416	0.0162052	9.9697e-05	0.0083185	0.0109885	0.00314805	87.2973	1.22778	883.60	m_2
0.596669	1.35912	213.109	0.0603718	0.990794	0.0128236	0.00319312	0.000904859	21.8366	0.462169	319.79	m_2
1.26038	0.941523	110.546	5.43846	0.861313	0.00485017	0.00871378	0.00046938	3.16157	867.214	25.59	m_1
1.08131	0.804582	6451.2	0.0357497	0.354901	0.00712895	0.0102584	0.0273918	273.147	0.0404952	Collision	m_1, m_{IMBH}
0.882019	0.543311	476.624	0.136031	0.156689	0.0093799	0.0135731	0.00202374	140.998	2.05667	325.14	m_2
1.21533	1.26615	116.869	0.773728	0.941982	0.00547495	0.00476602	0.000496225	56.9765	1.5477	103.66	m_1
1.12682	0.658795	113.667	3.2672	1.23743e-06	0.00659069	0.0120092	0.000482631	6.63023	66.0148	34.09	m_1
0.558931	0.950102	112.397	8.1263	0.587741	0.013348	0.00861785	0.000477236	6.48808	98.3992	23.05	m_2

Table B.1: Full table of initial values of all 27 WD binaries that were run with our simulation as well as the outcome.

Appendix C

Additional Figures

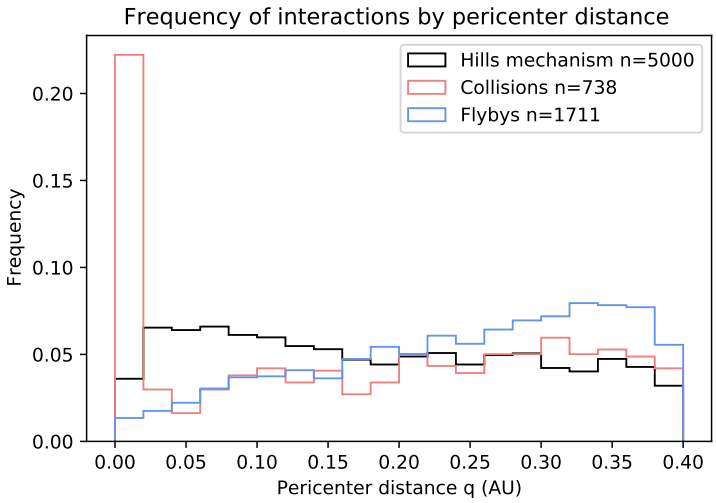

Figure C.1: Number of interactions by the pericenter distance q. Corresponding to Fig. 3.7

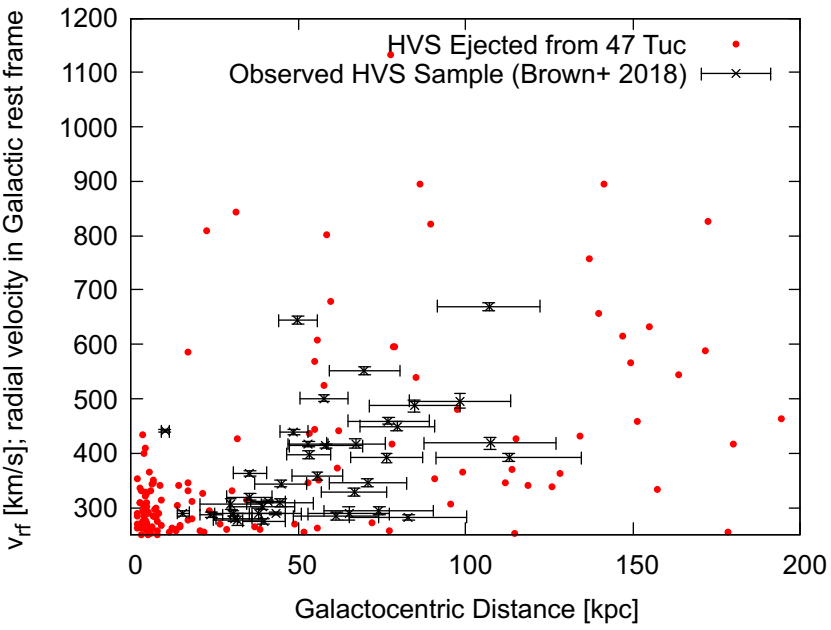

Figure C.2: Galactocentric distance vs Galactic rest frame radial velocities for sample of HVSs that were ejected out of 47 Tuc (red points) compared with observed HVSs from Brown et al. (2018).